Mineralogical Magazine, April 2004, Vol. 68(2), pp. 279–300

Dedicated to the memory of Dr A. J. Criddle, Natural History Museum, London, who died in May 2002

Micron- to nano-scale intergrowths among members of the cuprobismutite series and paděraite: HRTEM and microanalytical evidence

C. L. Ciobanu[1,*], A. Pring[2,3,4] and N. J. Cook[1]

[1] Geological Survey of Norway, N-7491 Trondheim, Norway
[2] South Australian Museum, North Terrace, Adelaide, South Australia 5000, Australia
[3] Department of Geology and Geophysics, University of Adelaide, North Terrace, Adelaide, South Australia 5005, Australia
[4] School of Chemistry, Physics and Earth Sciences, The Flinders University of South Australia, GPO Box 2100 Adelaide, South Australia 5001, Australia

ABSTRACT

Coherent intergrowths, at the lattice scale, between cuprobismutite (N = 2) and structurally related paděraite along both major axes (15 Å and 17 Å repeats) of the two minerals are reported within skarn from Ocna de Fier, Romania. The structural subunit, DTD, 3 layers of paděraite, is involved at interfaces of the two minerals along the 15 Å repeat, as well as in transposition of 1 paděraite unit to 2 cuprobismutite units along the 17 Å repeat in slip defects. Lattice images obtained by HRTEM across intervals of 200–400 nm show short- to long-range stacking sequences of cuprobismutite and paděraite ribbons. Such nanoscale slabs mimic μm-scale intergrowths observed in back-scattered electron images at three orders of magnitude greater. These slabs are compositionally equivalent to intermediaries in the cuprobismutite-paděraite range encountered during microanalysis. Hodrushite (N = 1.5) is identified in the μm-scale intergrowths, but its absence in the lattice images indicates that, in this case, formation of polysomes between structurally related phases is favoured instead of stacking disorder among cuprobismutite homologues. The tendency for short-range ordering and semi-periodic occurrence of polysomes suggests they are the result of an oscillatory chemical signal with periodicity varying from one to three repeats of 15 Å, rather than simple 'accidents' or irregular structural defects. Lead distribution along the polysomes is modelled as an output signal modulated by the periodicity of stacking sequences, with Pb carried within the D units of paděraite. This type of modulator acts as a patterning operator activated by chemical waves with amplitudes that encompass the chemical difference between the minerals. Conversion of the paděraite structural subunit DTD to the C unit of cuprobismutite, conserving interval width, emphasizes that polysomatic modularity also assists interference of chemical signals with opposite amplitudes. Observed coarsening of lattice-scale intergrowths up to the μm-scale implies coupling between diffusion-controlled structural modulation, and rhythmic precipitation at the skarn front during crystallization.

Keywords: cuprobismutite, paděraite, HRTEM, stacking disorder, polysomatism, Ocna de Fier, Romania.

Introduction

As analytical methods have evolved in the past decades, a comprehensive systematic classification of modular structures has been established covering a broad spectrum of mineral groups, e.g. silicates, sulphosalts and other complex sulphides (e.g. Merlino, 1997, and references therein). Members of most sulphosalt series, and the bismuth sulphosalts (Bi-ss) in particular, are derived from archetypal modules (e.g. PbS, SnS)

* E-mail: cristiana.ciobanu@ngu.no
DOI: 10.1180/0026461046820187

and form coherent accretional (polysomatic) series that may be related one to another in a hierarchical manner (e.g. Makovicky, 1997*a*). According to Makovicky (1981), homology/polysomatism in a broader sense within Pb-Bi-sulphosalts is realized by building operators that allow combinations between octahedral $(111)_{PbS}$-like layers ('H' layers) and pseudotetragonal $(100)_{PbS}$-like layers ('T' layers).

At odds with such highly constrained and predictable crystal-chemical variation (e.g. rigorous substitution lines within the PbS-Bi_2S_3-Ag_2S compositional triangle for the lillianite and pavonite homologous series; e.g. Makovicky and Karup-Møller, 1977; Makovicky, 1979), are the extensive compositional fields reported for many natural Bi-ss specimens, and also the broad solid-solution ranges obtained in experimental studies (e.g. Springer, 1971; Mariolacos, 2002). The extent of, and reasons for, non-stoichiometry among Bi-ss (e.g. Mozgova, 1985) remains an open question. Non-stoichiometric compositions are often dismissed as being due to analytical errors or fine microscopic-scale intergrowths that were overlooked. Examination of apparently homogenous samples, by HRTEM revealed lattice-scale disordered intergrowths among members within the two most common Bi-ss series: bismuthinite derivatives in the aikinite-krupkaite range (Pring and Hyde, 1987; Pring, 1989) and lillianite homologues (Pring *et al.*, 1999).

Synthetic work in the PbS-Bi_2S_3-(Ag_2S) system, combined with HRTEM, has enabled the documentation of defect structures and stacking disorder within an accretional series (i.e. the lillianite series; Tilley and Wright, 1982; Prodan *et al.*, 1982; Skowron and Tilley, 1986, 1990). Similarly, annealing experiments on synthetic hammarite ($Cu_2Pb_2Bi_4S_9$) have shown that the state of cation ordering and formation of polysome strips progresses with cooling (Pring, 1995). Together, these studies illustrate that stacking disorder rather than simple substitutional solid solution is currently a more favoured mechanism to explain compositional fields within both of these series. Moreover such nanoscale intergrowths can occur between members of different but closely structurally related series, for example between cosalite and lillianite homologues (Pring and Etschmann, 2002).

In this paper we report on disordered intergrowths among members of the cuprobismutite series and the related species, paděraite. Even though cuprobismutite homologues and/or paděraite have been mentioned from a total of 13 localities, there remains considerable ambiguity regarding the identity of these minerals, the extent of solid-solution ranges or substitution mechanisms. In our material from skarn ore from Ocna de Fier, southwest Romania (Cook and Ciobanu, 2003), the presence of intergrowths has been identified at scales differing by three orders of magnitude (from micron- to nanoscale). Such an 'intergrowths-upon-intergrowths' assemblage represents the first such documented example among Bi-sulphosalts, and closely mirrors that known for biopyriboles and humite groups (Veblen *et al.*, 1977; Veblen and Buseck, 1979; White and Hyde, 1982*a*,*b*). We address the question as to whether this type of coarsening of lattice-scale intergrowths up to the μm-scale is related to the diffusion-controlled patterning phenomena that often occurs in skarn systems (Ciobanu and Cook, 2000, 2004).

The cuprobismutite series and related paděraite

The cuprobismutite homologous series has the general structural formula: $Cu_8Me^{(quasi)octahedral}_{4(N-1)+2}Bi_8^{square\ pyramidal}S_{4N+16}$ (Makovicky, 1989) and includes three recognized minerals and two synthetic compounds (Table 1). Even though the cuprobismutite series is not part of the Pb-Bi sulphosalt group *sensu stricto*, the structures can be considered in terms of the periodic intergrowth of $(331)_{PbS}$-like octahedral layers with layers of metals in tricapped trigonal-prismatic coordination (Makovicky, 1989). Each member contains a layer with Cu atoms linked with chains of Bi_2S_4, the so-called 'C' layer, common to all members. These layers alternate with a second type of layer where Cu atoms are linked to ribbons of Bi with octahedral and square-pyramidal coordination. Incremental width variation of this second layer, achieved by the addition of more square-pyramids of Bi accounts for accretional homology between members with integer N number within the series (Koděra *et al.*, 1970; Ozawa and Nowacki, 1975; Mariolacos *et al.*, 1975). Makovicky (1997*b*) describes polysomatism within the cuprobismutite series as coherent intergrowths of incremental octahedral slabs with trigonal prismatic slabs (Table 1, Fig. 1*a*); and denoted the species by: N_1, N_2 = (1,1), (1,2), (2,2).

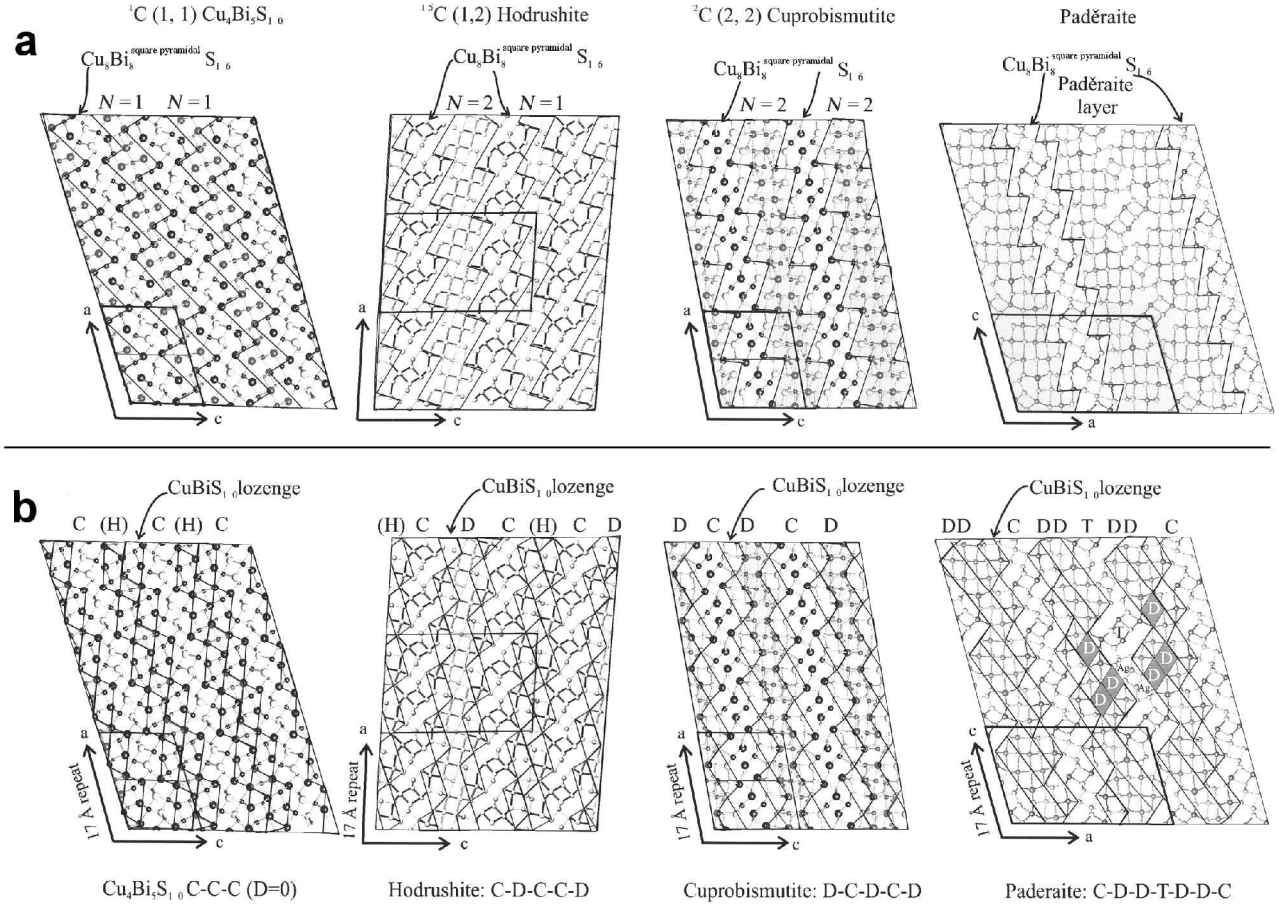

FIG. 1. The cuprobismutite series and related paděraite, according to (*a*) Makovicky (1989) and (*b*) Mumme (1986). Paděraite shares the common $Cu_8Bi_8S_{16}$ layer with members of the cuprobismutite series. In the paděraite structure (*b*, right), the D module has variable thickness along the *c* axis: either one octahedron thick at the T contact, or two octahedra thick along the trigonal-tetrahedral match. In each drawing, atoms are, in decreasing size, S, Bi and Cu. In the drawings for paděraite, the order is Pb, S, Bi, Ag and Cu.

TABLE 1. Natural occurrences and mean compositions of cuprobismutite homologues and paděraite.

ineral	Ideal formula	Locality	Cell dimensions (Å)			Angle	Space group	Nomenclature				Reference
								Makovicky (1989)		Mumme (1986)		
	Empirical formulae to corresponding number of atoms p.f.u.		a	b	c			^{N}C (*N*1+*N*2)/2	Combinatorial (*N*1,*N*2)	Layers (C,D)	Sequences	
uprobismutite series	$Cu8Me^{(quasi)octahedral}_{4(N-1)+2}Bi_8^{square\ pyramidal}S_{4N+16}$											
deal	$Cu_8Bi_{10}S_{20}$							^{1}C	(1, 1)	^{1}C^{0}D	(-1C-0D-1C-0D-1C-)	
ynthetic	$Cu_4Bi_5S_{10}$		17.54	3.93	12.85	108.0	*C*2/*m*					Mariolacos *et al.* (1975)
upčikite	$Cu_{6.8}Fe_{1.2}Bi_{12}S_{20}$	Felbertal, Austria										Topa (2001)
deal	$Cu_8Bi_{12}S_{22}$							$^{1.5}$**C**	**(1, 2)**	**^{2}C^{1}D**	(-1C-1C-1D-1C-1C-)	
	$(PbAgBi)Cu_4Bi_5S_{11}$											Kupčik and Makovicky (1968)
odrushite	$Cu_{8.12}Fe_{0.29}Bi_{11.54}S_{22}$	Hodrušha, Slovakia	17.58	3.93	27.21	92.2	*C*2/*m**					Koděra *et al.* (1970)
	$(Cu_{7.55}Fe_{0.36})_{7.91}(Ag_{0.39}Bi_{11.58})_{11.97}S_{22.11}$	Felbertal, Austria										Topa (2001)
	$(Cu_{7.8}Fe_{0.23})_{8.03}(Ag_{0.35}Pb_{0.12}Bi_{11.5})_{11.97}S_{21.99}$	Ocna de Fier, Romania										Cook and Ciobanu (2003)
	$Cu_{8.28}Fe_{0.32}Bi_{11.54}S_{21.8}$ (36p)	Swartberg, South Africa										Ciobanu *et al.* (2002*a*)
deal	$Cu_8Bi_{14}S_{24}$							^{2}**C**	**(2, 2)**	**^{1}C^{1}D**	(-1D-1C-1D-1C-1D-)	
ynthetic	$Cu_{10.4}Bi_{12.6}S_{24}$		17.52	3.926	15.261	100.18	*C*2/*m*					Ozawa and Nowacki (1975)
uprobismutite	$Cu_{20.75}Ag_{0.97}Pb_{0.35}Mn_{0.22}Bi_{26.66}S_{50.38}Se_{0.55}$	Tunnel Ext.Mine 2,	17.628	3.911	15.19	101.16	C2/m,C2,Cm					
aylor *et al.* (1973)		Ohio, USA										
uprobismutite	$Cu_8(AgBi_{13})_{14}S_{24}$											
	$Cu_{8.04}(Ag_{1.04}Bi_{12.85})_{13.89}S_{24.07}$	Felbertal, Austria										Topa (2001)
	$Cu_{8.07}(Ag_{0.99}Pb_{0.2}Bi_{12.72})_{13.91}S_{24}$	Ocna de Fier, Romania										Cook and Ciobanu (2003)
deal	$Cu_8Bi_{16}S_{26}$							$^{2.5}$**C (?)**	**(2, 3) (?)**			
nnamed phase (ideal)	$Cu_8Ag_2Bi_{14}S_{26}$											
nnamed phase (empir.)	$Cu_{7.94}Ag_{1.91}Pb_{0.21}Bi_{13.76}S_{26.17}$	Vurli Bryag, Bulgaria										Ciobanu *et al.* (2002*b*)
aděraite tructural formula	$Cu_6AgPbBi_{12}S_{22}$		28.44	3.9	17.55	106	*P*21/*m*			^{1}C^{d}D	(-4D-1C-4D-1C-4D-)	Mumme (1986)
mpirical formula	$Cu_{5.9}Ag_{1.3}Pb_{1.6}Bi_{11.2}S_{22}$	Báiţa Bihor, Romania										Mumme and Žák (1985)
	$Cu_{7.11}Ag_{0.36}Pb_{1.2}Bi_{11.28}S_{22.05}$	Ocna de Fier, Romania										Cook and Ciobanu (2003)
	$Cu_{7.36}Pb_{1.31}Bi_{11.32}S_{22}$	Swartberg, South Africa										Ciobanu *et al.* (2002*b*)

as given by Mariolacos *et al.* (1975)

Mumme (1986) described the structurally related phase, paděraite, ($Cu_{5.5}Ag_{1.1}Pb_{1.2}Bi_{11}S_{22}$; Mumme and Žák, 1985) and although Pb-bearing, paděraite has unit-cell dimensions closely resembling those of hodrushite, a member of the cuprobismutite series (Kupčik and Makovicky, 1968). The structural refinement for paděraite was based upon a slightly different chemistry: an ideal formula of $Cu_6AgPb_2Bi_{11}S_{22}$, assuming a ratio of *Me*:S equal to 20:22, rather than 19:22 derived from the empirical formula. The formula was recalculated by Mumme (1986) to give $Cu_{5.9}Ag_{1.3}Pb_{1.6}Bi_{11.2}S_{22}$, thus matching both the charge balance and structural data.

Mumme (1986) stressed common 17.5 Å repeats for all phases within the cuprobismutite series and in paderaite. This 17.5 Å repeat is given by two $CuBiS_{10}$ lozenges arranged *en echelon* at the margins of the C layer (with pairs of Bi_2S_7 and CuS_4 groups in the middle). These lozenges consist of pairs of BiS_6 octahedra attached to a square pyramidal Cu; seen in each of the structures under consideration (Fig. 1*b*). Mumme (1986) discussed the layer realized by insular octahedra (H configuration) which links the C layers in hodrushite and $Cu_4Bi_5S_{10}$. We will denote this as (H). Differences among individual members of the cuprobismutite series are achieved by the presence (or absence) of another layer, the 'D' layer, a one octahedron (H configuration) wide strip that follows lozenges *en echelon* parallel to $(331)_{PbS}$. A further difference is the distinct stacking combinations between C and D layers (Fig. 1, Table 1). At the inner part of the double C layers, as found in $Cu_4Bi_4S_{10}$ and hodrushite, arrays of insular H octahedra [C(H)C] are present. In such an approach, the structure of $Cu_4Bi_5S_{10}$ is a sequence of C(H)C(H) layers (with no D layer); cuprobismutite consists of alternating DCDCD layers, whereas hodrushite is a sequence of (H)CDC(H)CD layers.

The D layer, parallel to $(331)_{PbS}$ is also in the paděraite structure, and this layer incorporates the Pb atoms. The D layer also incorporates Cu atoms, which are not part of the C layer (Fig. 1*b*). The Pb atoms have distorted octahedral coordination that can be considered as sheared pseudo H-layers [$(111)_{PbS}$]. There are two modules of 2D layers, even though each of them has a variable 1–2 octahedra thickness (Fig. 1*b*). These are separated by a T layer, which has a $(100)_{PbS}$-like structure and contains Bi_4S_{12} strips with adjacent trigonally co-ordinated Cu. These Bi_4S_{12} strips are linked along the *c* axis by pairs of AgS_4 tetrahedra. Therefore, along the *c* axis the D module is either one octahedron thick at the T contact, or two octahedra thick along the trigonal-tetrahedral match. The difference between hodrushite and paděraite can thus be defined in a polysomatic manner (Fig. 1*b*), on the basis of the layer stacking sequence; paděraite is TDDCDDTDDC. Therefore, paděraite has a similar repeat to cuprobismutite (DCD), whereas hodrushite includes the double C repeat 'C-C' linked by D layers; i.e. CCDCCDCC (Table 1).

Sample description

The material used in this study comes from Paulus Mine, in the northern part of the 76.5 Ma Fe-(Cu)-(Zn-Pb) skarn at Ocna de Fier, southwest Romania (Ciobanu *et al.*, 2002*a*). The locality is known for the occurrence of bismuth sulphosalts, and especially for specimens consisting of fine intergrowths, e.g. co-type samples of 'rezbanyite' (Zák *et al.*; 1992). In this new Paulus occurrence (the mineral collector Constantin Gruescu discovered this occurrence during the 1980s), dense pockets of Bi-ss form swarms within an area several metres in width in massive magnetite ore on the 206 m mining level. Intergrowths are abundant and have varied morphologies. The intergrowths span the bismuthinite derivative series and occur with makovickyite and galenobismutite (Ciobanu and Cook, 2000). Cook and Ciobanu (2003) reported compositional and textural data for cuprobismutite, paděraite and occasional hodrushite from an individual pocket, several cm in size, from the same occurrence.

As seen in Table 1, the empirical formulae for paderaite from Ocna de Fier, calculated for 42 a.p.f.u., is close to the ideal $Cu_7(Ag,Pb)_2Bi_{11}S_{22}$, thus differing from TL paděraite (ideal $Cu_6AgPb_2Bi_{11}S_2$) with respect to the Cu:Ag:Pb ratio. The *Me*:S ratio, however, is close to 20:22, the ratio used for the structural refinement. A similar formula for paděraite, close to ideal $Cu_7(Cu,Pb)_2Bi_{11}S_{22}$, was obtained for material from another locality (Swartberg, South Africa; Table 1; Ciobanu *et al.*, 2002*b*). This allows us to speculate that the number of Pb atoms in paděraite might be fixed at 2 (at 42 a.p.f.u.), while Ag can be absent. Variation in the Cu:Ag:Pb ratio can be written as a substitution mechanism Ag(Cu) + Bi $\rightleftharpoons$ 2Pb. Further variation of the Cu:Bi ratio, beyond a fulfilment of Pb positions, would imply structural modifications and indicate a possible

paděraite series (Ciobanu *et al.*, 2002*b*). However, a structural refinement of Ag-free paděraite is required to substantiate this hypothesis.

Cuprobismutite, the most abundant phase in the material, tends to develop thin prisms (5–10 μm) with pyramidal termination (Fig. 2*a*). It also occurs as narrow bands within a matrix of finely intergrown, and apparently homogeneous 'patches' having an intermediate composition between paděraite and cuprobismutite (Fig. 2*b*). However, more common are aggregates of cuprobismutite homologues with paděraite (CBP; Fig. 2*c*), 100–200 μm in diameter, with angles of 90–120º between laths randomly distributed within a coarse-grained matrix of oversubstituted bismuthinite (BD_{10} – the BD index represents the aikinite number calculated after Makovicky and Makovicky (1978)). Minor hodrushite is occasionally included in the aggregates (Fig. 2*d*). The stepwise arrangement of laths within some of the orthogonal CBP aggregates, with lath-width reducing towards the interior of the aggregates, suggests similarities with patterns developed during skeletal growth. Cuprobismutite has a strong idiomorphic tendency where formed against laths dominated by paděraite compositions (Fig. 2*e*). Lamellae within CBP aggregates mainly consist of alternating cuprobismutite and paděraite (Fig. 2*f*).

Makovickyite is almost always present in small quantities between lamellae of CBP. In contrast to the entire occurrence in Paulus, in this particular suite of samples, the compositional range of the bismuthinite derivatives is restricted to a limited range between gladite and bismuthinite (BD_{33}-BD_{2-3}). Krupkaite and coarse gladite-krupakaite intergrowths are also observed in minor amounts. In reflected light, equilibrium crystal boundaries with 120º triple joint points are commonly observed between BD_{10} grains.

Micron-scale intergrowths

There are well-defined compositional variations between certain minerals in individual aggregates. Even though hodrushite is part of these aggregates, intermediate composition intervals are in the cuprobismutite-paděraite range rather than the cuprobismutite-hodrushite range. The orthogonal CBP aggregates (Fig. 2*c*) are formed by laths 40–60 μm wide, which consist of alternating sequences of cuprobismutite (Cbs) and either paděraite (Pad) or mixed ('Mix') domains with intermediate compositions between the two minerals.

Two such sequences are shown in Fig. 2*e* and *f*, across laths of 55–60 μm within CBP. In both cases, an interval 5 μm wide represents the stepwise variation of Pb between 1 wt.% (Cbs) and 6–7 wt.% (Pad). This interval is also seen as the smallest width of individual cuprobismutite needles (Fig. 2*a*). The 'Mix' interval is found instead of either one or the other mineral in a regular Cbs.Pad.Cbs.Pad sequence (Fig. 2*e*), or as a shoulder between intervals of Cbs and Pad (Fig. 2*f*). If the differences in wt.% Pb between two consecutive intervals are plotted (dPb; Fig. 2*g*,*h*), we obtain, in both cases, a bimodal variance across the entire sequences. The first sequence is more regular, with dPb = 3 wt.%, whereas the second sequence combines two steps of dPb = 3 wt.% and dPb = 6 wt.%, respectively. This bimodal inversion of the Pb gradient across individual laths can be considered as the most contrasting chemical signal controlling the appearance of μm-scale intergrowths within CBP.

FIG. 2. (*facing page*) BSE images showing cuprobismutite homologues and paděraite. (*a*) Needles (5-10 μm) of cuprobismutite (Cbs) with pyramidal termination. The matrix consists of over-substituted bismuthinite (BD_{10}) with fields of fine intergrowths. The average composition within such fields is in the range between gladite and pekoite ($BD_{32\text{-}16}$). (b) Area with mixed composition between paděraite (Pad) and Cbs. Several narrow bands with Cbs composition are seen in the middle part. (*c*) Orthogonal aggregates of cuprobismutite-paděraite (CBP) in a matix of BD_{10}. Note the stepwise arrangement of laths, with lath-width reducing towards the interior of the aggregate. Makovickyite (Mak) and gladite (Gl) are seen as darker shades than the matrix between the laths. (*d*) Hodrushite (Hod) and Cbs in a lath dominated by Pad. (*e* and *f*) Details of laths within cuprobismutite-paděraite aggregates (CBP) showing Pb (wt. %) variance across sequences of alternating cuprobismutite (noted as 'C'), paděraite ('P') and mixed material in the Cbs-Pad range ('M'). In (*e*), the lower marginal needle of Cbs crosscuts the boundary of makovickyite (Mak) towards BD_{10}. The points mark the line of the profile. (*g* and *h*) Diagrams showing the bimodal variance of Pb (in wt.%) across the sequences in (*e*) and (*f*), plotted as difference between two adjacent intervals of 5–10 μm each.

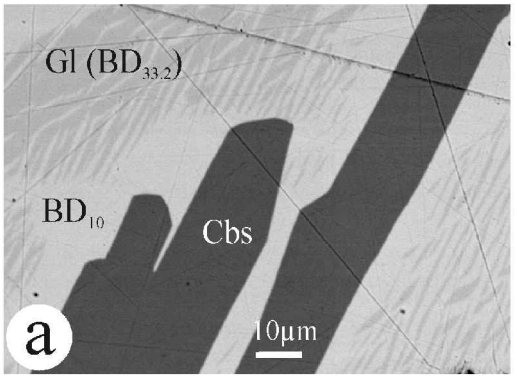
Gl (BD33.2)
BD10
Cbs
10µm
a

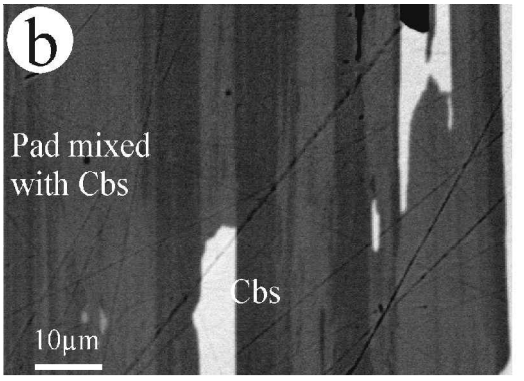
b
Pad mixed
with Cbs
Cbs
10µm

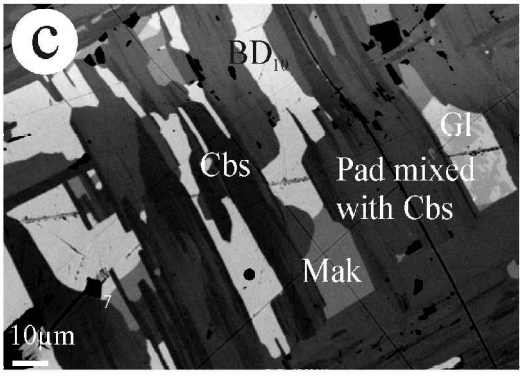
c
BD10
Gl
Cbs
Pad mixed
with Cbs
Mak
10µm

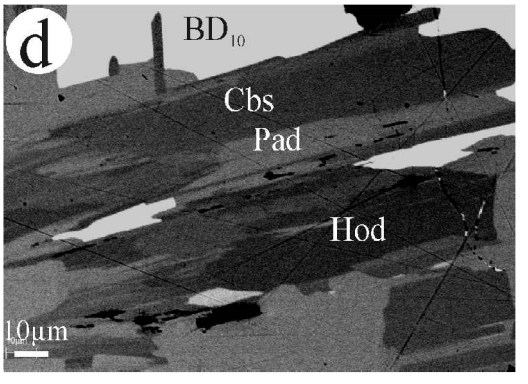
d
BD10
Cbs
Pad
Hod
10µm

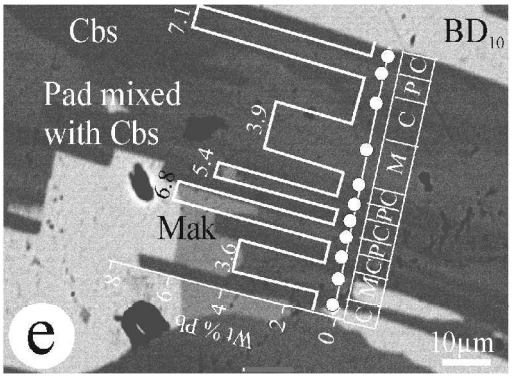
Cbs
BD10
Pad mixed
with Cbs
Mak
7.1
3.9
5.4
6.3
3.6
3.7
Wt % Pb
10µm
e

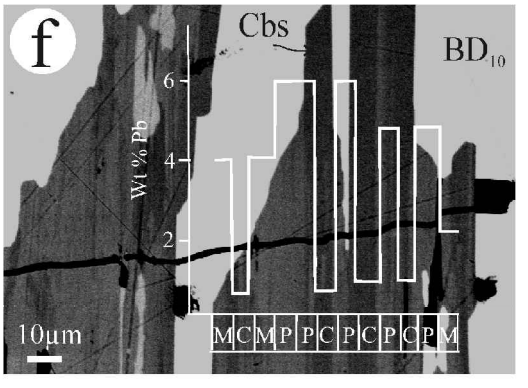
f
Cbs
BD10
Wt % Pb
10µm
M C M P P C P C P C P M

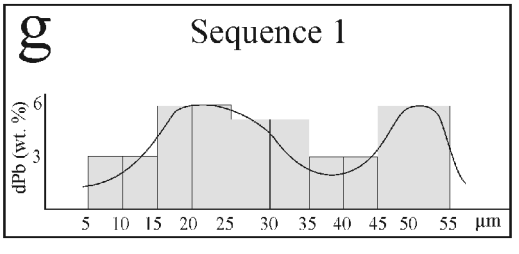
g
Sequence 1
dPb (wt. %)
5 10 15 20 25 30 35 40 45 50 55 µm

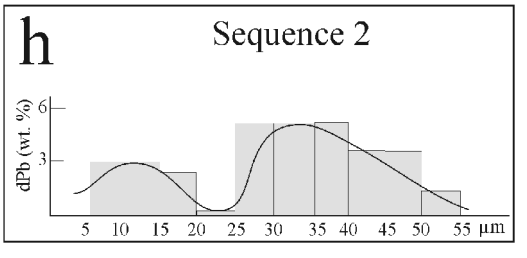
h
Sequence 2
dPb (wt. %)
5 10 15 20 25 30 35 40 45 50 55 µm

Similarly, the bismuthinite derivatives in the sample also display a wide range of μm-scale intergrowths. Here, the observed lamellae are even smaller than in cuprobismutite, not exceeding 1–2 μm in width. Commonly, fields of fine pencil-like intergrowths of $BD_{32\text{-}17}$ are nested within rectangular aggregates of CBP. Between the two phases at the ends of the compositional range, i.e. BD_{10} and BD_{32}, there is a four-fold difference in Pb (3 *vs.* 12 wt.%), coupled with a three-to four-fold difference in Cu (1.2 *vs.* 4.3 wt.%). However, an intermediate composition, BD_{17}, may correspond to the finest lamellae within the intergrowths fields rather than gladite (BD_{32}). Such a composition would give appreciably smaller ratios (a factor of two) for Pb (3 *vs.* 6 wt.%) and (Cu 1.2 *vs.* 2 wt.%) compared to BD_{10}. Wider lamellae of gladite are meshed across these fields, or outline the margin of makovickyite. Gladite also occurs as larger grains, 50–100 μm in diameter, enveloped by halos consisting of lamellar intergrowths dissipating within the matrix. Rarely, at the inner part of such gladite grains, cores of krupkaite composition are observed that dissipate into gladite. Surprisingly, makovickyite is homogenous (Cu, Ag and Pb = 5, 5 and 2 wt.%) in the assemblage, even though this phase is known for its abundant basket-weave intergrowths (e.g. Žák *et al.*, 1994).

Methodology

Electron microscopy

Several fragments of the Bi-ss material were taken from the same sample that provided the polished blocks (GS) analysed previously (Cook and Ciobanu, 2003). The fragments were ground under acetone in an agate mortar and the resultant suspension was dispersed on Cu grids coated with holey-carbon support films. The grids were analysed using a 200 kV Philips CM200 electron microscope fitted with a standard side-entry goniometer (±60º), objective lens with C_s = 2.00 mm and a W filament. This configuration gives a point-to-point resolution of 2.8 Å. The crystal fragments seen over the holes in the film were tilted into the [010] zone. Lattice images and diffraction patterns were taken at 250,000× magnification using exposure times of 2–4 s. A series of image simulations was performed by the conventional multi-slice method, using local programs based on the routines by G.R. Anstis and T.B. Williams (pers. comm.) in order to establish the criteria for image interpretation.

Results

In Fig. 3*a*, we show an electron diffraction pattern for cuprobismutite down to [010], corresponding to the lattice images in Figs 3*b* and 4*b*. The pattern shows a net, 1/9.75 and 1/7.75 $Å^{-1}$ in size, at an angle of 100º, however the absences due to the space group *C*2/*m* are such that only rows with $h = 2n$ are present. The streaking along the main rows in the diffraction pattern, and the weak streaked lines of intensity between the main *h*0*l* rows are both due to the disordered intergrowth of paděraite.

Individual or paired satellite reflections visible in the diffraction pattern correspond to the paděraite cell. The relationship between the diffraction patterns is $a_{cbs} \parallel c_{pad}$ and a_{pad} is rotated 6º from c_{cbs}. The streaking in the diffraction pattern is due to lattice-scale disorder seen in the images (Figs 3*b* and 4*b*). These lattice images show thicker and brighter rows due to paděraite within cuprobismutite (Figs 3*b* and 4*b*). Interpretation of the images is verified by computer simulation of paděraite and cuprobismutite (down to [010]; Fig. 4*b*, insets). Differences between the appearance of the paděraite strips in Figs 3*b* and 4*b* are due to the variable thickness of the crystals; at the left side of Fig. 4*b* several rows of paděraite appear as in Fig. 3*b*.

Nano-scale intergrowths

The lattice images (Figs 3*b* and 4*b*) represent intervals of 370 and 270 nm, respectively, with intergrowths on the scale of 10 to 100 Å, i.e. three orders of magnitude smaller than the 5 μm interval observed for the variation of Pb and Ag across CBP laths by microanalysis. Even though intergrowths <~1 μm are beyond microanalytical resolution limits of scanning electron microscope and microprobe techniques, they can nevertheless be distinguished in back-scattered electron images of mixed material with compositions intermediate between cuprobismutite and paděraite, especially at the boundary between two different compositional domains (e.g. Fig. 2*b*,*e*). Alternatively, a compositional transition can be seen in larger domains (~20–30 μm wide), when the Pb/Ag bimodal inversion takes place across a couple of strongly contrasting, 5 μm wide lamellae, i.e. Fig. 3*a*, Table 2. We assume that both styles of transition observed within domains of intermediate composition can include lattice-scale

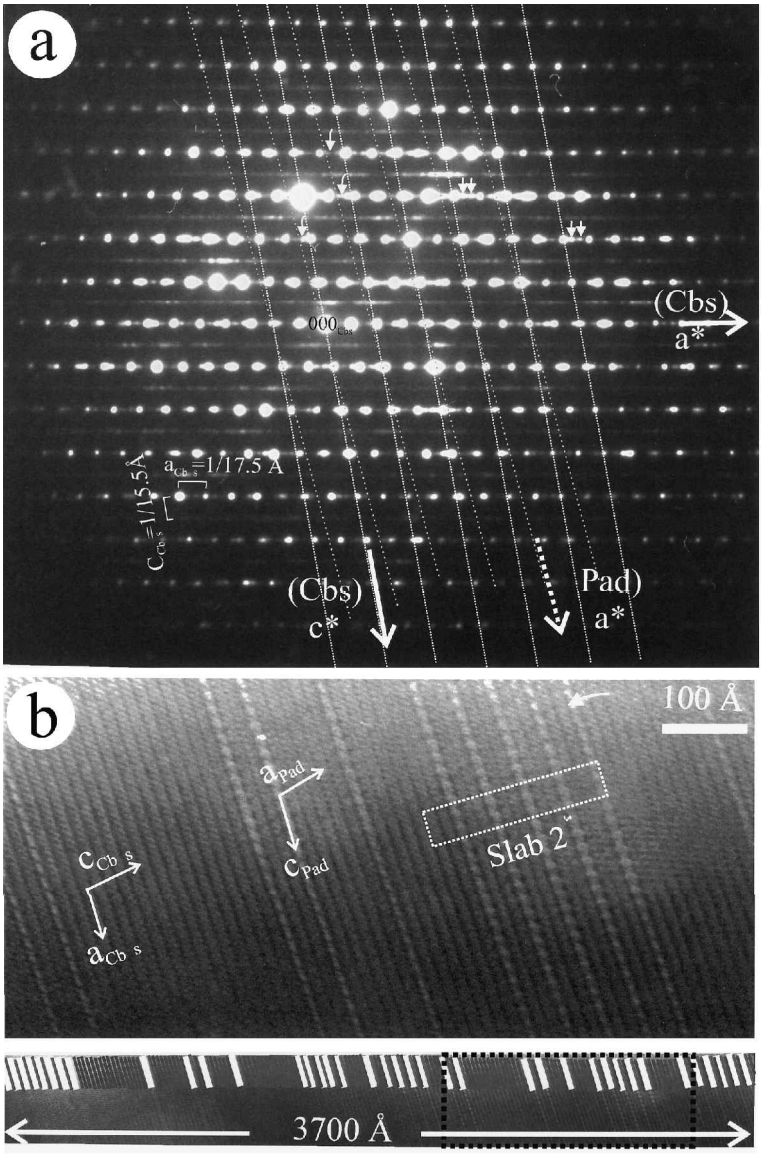

FIG. 3. (*a*) Electron diffraction pattern of cuprobismutite (Cbs) down [010]. Note slight streaking along the *a** axis, due to intergrowths with paděraite (Pad). Satellite reflections corresponding to paděraite are arrowed. (*b*) High resolution transmission electron microscopy image of cuprobismutite with strips of paděraite (arrowed). The intergrowths are along the *c* axis of cuprobismutite and the *a* axis of paděraite (17 Å repeat axis). The white box marks the sequence: 5×2Cbs.Pad (Slab 2) as characteristic for disordered Cbs (see text). The image corresponds to the black box indicated on the low magnification strip at the bottom of the figure. Here we see a tendency towards a banding induced by variable combinations of Pad.$(N_{Cbs})_{1\text{-}3}$.Pad modules. The modules are shown as white (Pad) and grey (Cbs) bands at the top of the strip.

disorder, as these are compositionally equivalent to intermediates in the cuprobismutite–paděraite range.

The lattice image in the lower part of Fig. 3*b* shows an area of intergrowths 370 nm wide, in which ¼ of the unit cells are paděraite (38 units)

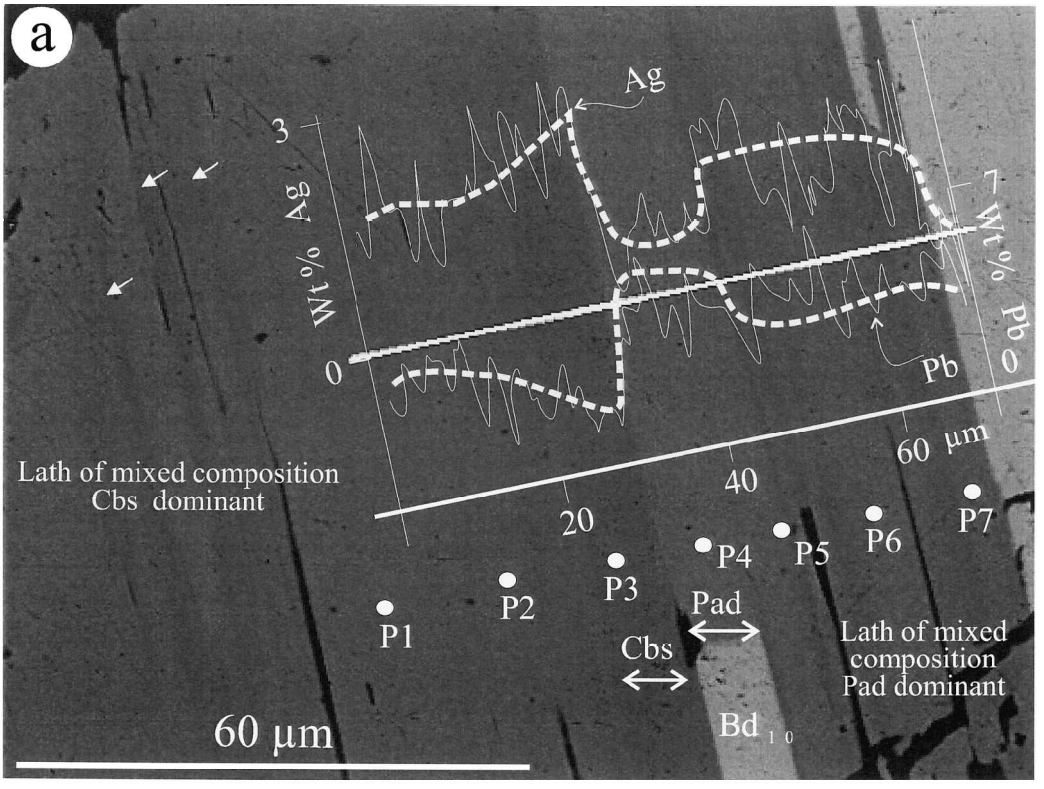
a
Ag
3
Wt% Ag
0
Wt% Pb
Pb
0
60 µm
Lath of mixed composition
Cbs dominant
20
40
P1
P2
P3
P4
P5
P6
P7
Pad
Cbs
Lath of mixed composition
Pad dominant
60 µm
Bd 10

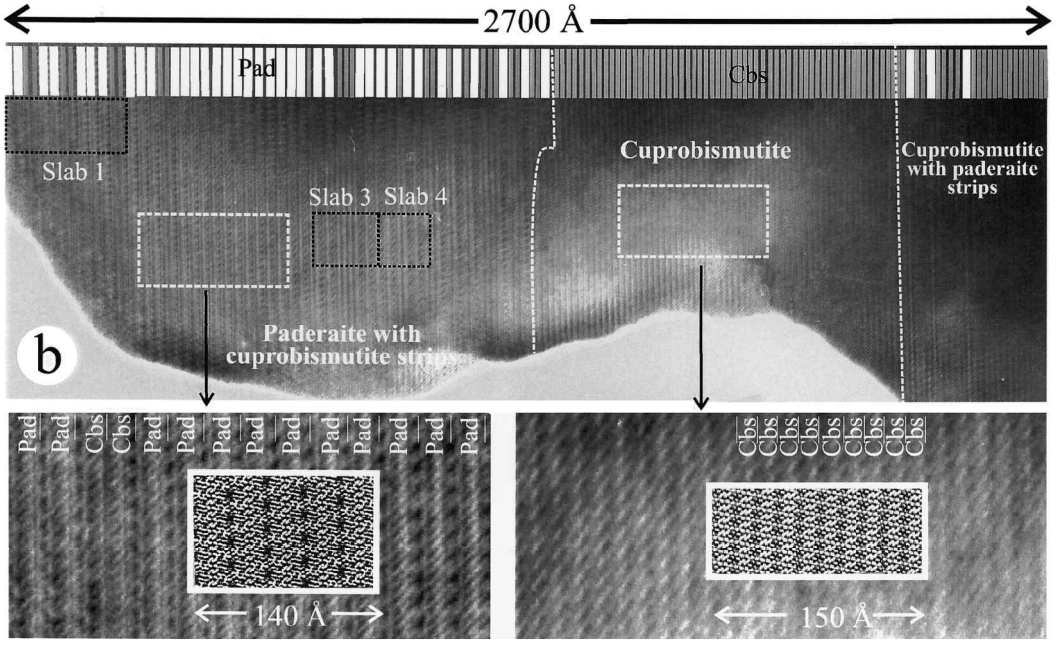
2700 Å
Pad
Cbs
Slab 1
Slab 3
Slab 4
Cuprobismutite
Cuprobismutite with paderaite strips
b
Paderaite with cuprobismutite strips
Pad
Cbs
140 Å
150 Å

TABLE 2. Compositions along the profile shown in Fig. 4*a*.

Element wt.%	Mixed P1	Mixed P2	Cbs P3	Pad P4	Mixed P5	Mixed P6	Mixed P7
Cu	11.80	11.90	12.10	11.40	11.80	11.50	10.60
Ag	**1.73**	**1.63**	**2.46**	**0.76**	**1.57**	**1.06**	**1.15**
Fe	0	0	0	0	0	0	0
Cd	0.30	0.30	0.30	0.20	0.20	0.20	0.30
Pb	**3.60**	**3.60**	**0.80**	**6.11**	**3.80**	**5.80**	**4.90**
Bi	64.00	63.50	65.20	60.80	63.60	62.20	63.90
S	18.10	18.90	18.90	18.40	18.30	18.50	18.40
Se	0	0	0	0	0	0	0.09
Total	99.53	99.83	99.76	97.67	99.36	99.26	99.34
Atomic proportions							
Cu	18.57	18.73	19.04	17.94	18.57	18.10	16.68
Ag	**1.60**	**1.51**	**2.28**	**0.70**	**1.46**	**0.98**	**1.07**
Fe	0	0	0	0	0	0	0
Cd	0.27	0.27	0.27	0.18	0.18	0.18	0.27
Pb	**1.74**	**1.74**	**0.39**	**2.95**	**1.83**	**2.80**	**2.36**
Bi	30.62	30.39	31.20	29.09	30.43	29.76	30.58
S(+Se)	56.46	58.95	58.95	57.39	57.19	57.70	57.51
Charge balance (%)	2.74	−2.14	−1.43	−2.30	0.84	−0.9	−0.24

within ¾ cuprobismutite (130 units). The paděraite units are scattered through the crystal in what appears to be a random manner. However, single isolated units of paděraite are rare; instead regular alternation of paděraite and cuprobismutite units is common, often in groups of 3 or 4 repeats. Sometimes, the units of paděraite are separated by two or even three cuprobismutite units. This suggests that ordered intergrowths of paděraite and cuprobismutite might occur and even be stable as long repeat homologues. Such intergrowth homologues would have the general form PadN_{Cbs}Pad, and the stacking of individual slabs can be written as **TD***DCD***DT**/(DCD)$_{1-3}$/**TD***DCD***DT**.

In order to achieve such a layer stacking, there are two possible ways to coherently intergrowth the layer sequences of paděraite and cuprobismutite. This first is through common D layers (Fig. 5*a*). The second is linking through common C layers (Fig. 5*b*,).

We draw attention to the fact that DCD sequences (in italics in the preceding formalism) that formalize cuprobismutite units are also found in the middle part of paděraite. Even though there are differences introduced by the peculiar 2D configuration in paděraite, their similarity permits a coherent stacking sequence. Therefore the lattice image can be interpreted as a regular matrix of DCDC..., with insertion of coupled DTD—DTD groups at intervals that vary as DCD, DCDCD, DCDCDCD within a $4 \times$ PadN_{Cbs}Pad slab.

In contrast, the lattice image in Fig. 4*b* shows an alternation of wider slabs of well-ordered

FIG. 4. (*facing page*) (*a*) BSE image showing micron-scale intergrowths between cuprobismutite (Cbs) and paděraite (Pad). Needles of Cbs within the lath with Cbs dominant composition are arrowed. Variation of Pb and Ag across an energy dispersive line scan is also shown. Bd_{10}: oversubstituted bismuthinite. The points 1–7 represent the location for the analyses in Table 2. (*b*) Lattice image showing styles of coherent intergrowth between paděraite (Pad) and cuprobismutite (Cbs); irregular strips of Cbs within a domain of Pad (to the left). At the top of the image the intergrowths sequence is shown as white (Pad) and grey (Cbs) bands. The sequences discussed in the text as Slab 1, 3 and 4 are marked in black boxes. Insets show details of Pad and Cbs with corresponding computer simulations down [010], at 900 Å defocus.

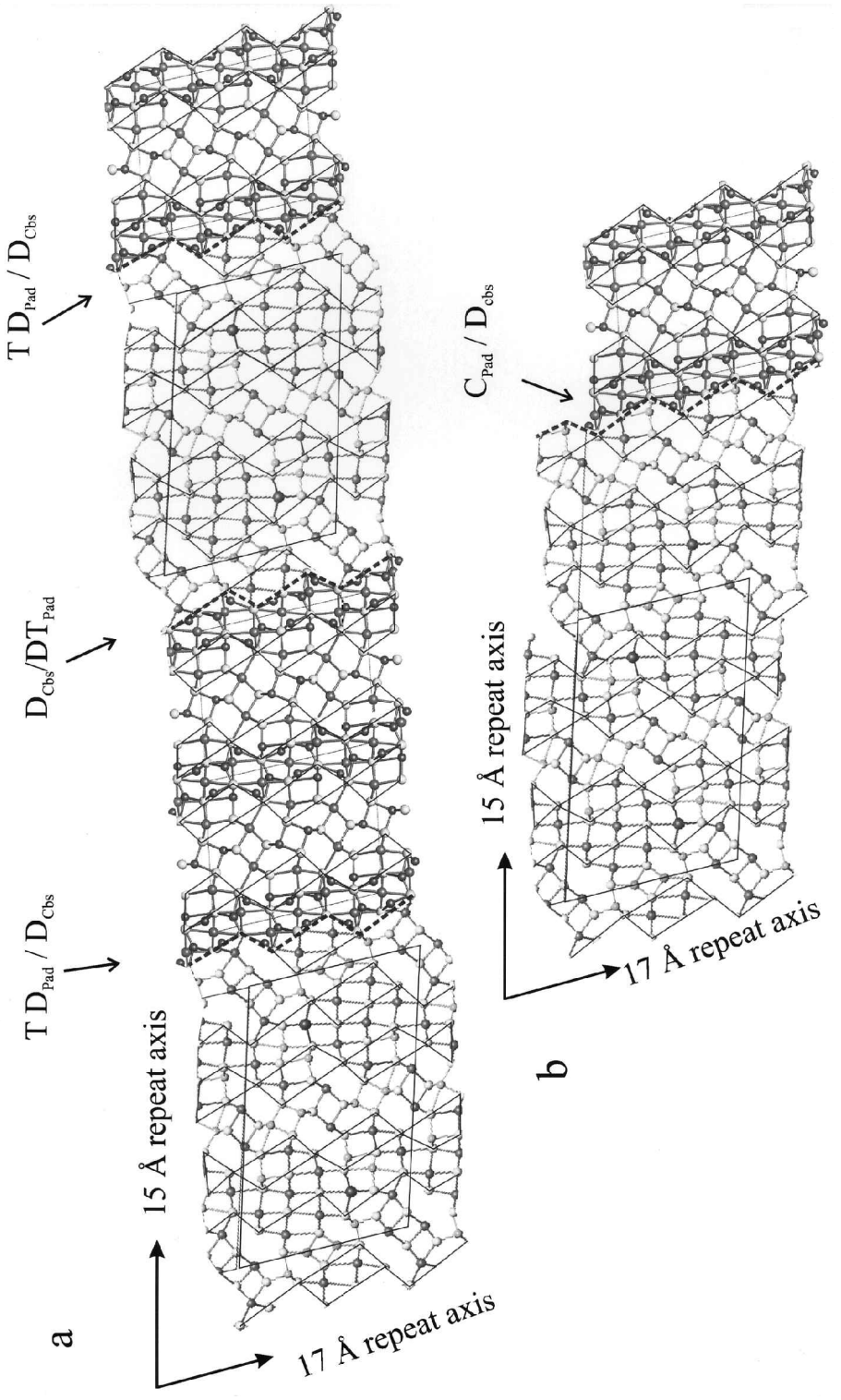

FIG. 5. Coherent intergrowths along the 15 Å repeat axis between slabs of paděraite and cuprobismutite through common D layers (*a*) or through common C layers (*b*). The layers and atoms are according to Fig. 1*b*.

paděraite and cuprobismutite (50–100 nm wide). Such a combination approximates the style of compositional variation shown in Fig. 4*a*, at scales differing by an order of magnitude.

The sequence shown in Fig. 4*b* shows three distinct intervals as follows: disordered paděraite, ordered cuprobismutite and disordered cuprobismutite (~140 nm, 100 nm and 30 nm wide, respectively). The disorder in paděraite is seen at both ends of the interval as insertion of cuprobismutite rows in repeats of 1–3 unit cells resembling similar PadN_{Cbs}Pad modules as in the previous image. However, ordered intergrowth sequences of paděraite and cuprobismutite (PadN_{Cbs}Pad modules) are absent and the intergrowths are more irregular. Nevertheless, a similarity to the previous case is seen in the partial short-range order of the modules at the left end of the interval, even though they here include repeats of PadN_{Cbs}PadPadN_{Cbs}Pad(N_{Cbs} = 1–3), which doubles the inner paděraite row in the sequence. Repeats that share the inner paděraite (T layer) unit are seen further to the right, at the end of paděraite to the boundary against ordered cuprobismutite.

The layer stacking for such a disordered paděraite sequence (2Pad/2Cbs/2Pad) reads as: **TD***DCD***DTD***DCD***DTD**DCDCD**DTD***DCD* **DTD***DCD***DT**. It consists of 6 unit cells combined with a ratio of 2:2 and 10 repeats of 3-layer modules (DCD, DTD, CDC) of ~15 Å wide each. We point to the fact that a repeat of CDC layers corresponding to a unit of hodrushite encompassed in a group of two cuprobismutite units within such modules, even though the image resolution does not allow us to discriminate between a D layer and a row of insular H modules. There is, therefore, a degree of uncertainty in this assumption.

The equivalent 10 repeats, (of the same 3-layer modules) sequence found in the disordered cuprobismutite with 1:2 ratio (Pad/2Cbs/Pad/2Cbs/Pad) reads: **TD***DCD***DTD**DCDCD**DTD** ***DCD*****DTD**DCDCD**DTD***DCD***DT** and encompasses 7 instead of 6 unit cells. In both of the sequences considered, the lattice disorder can be seen as regular insertion of a DTD type of module (with TD_{Pad}/D_{Cbs} and D_{Cbs}/DT_{Pad} at Pad/Cbs joints) in a matrix where DCD and CDC modules alternates by rhythms of 2:1 (paděraite) or 1:1 (cuprobismutite), respectively. Bearing in mind that the Pb atoms are included in the D layer adjacent to T, recognition of such DTD modules as markers for the state of disorder in the cuprobismutite-paděraite range has implications for defining the smallest intervals that can be associated with Pb distribution during diffusion-controlled crystallization, growth or reaction.

Using average compositions for cuprobismutite and paděraite at Ocna de Fier, we can calculate the compositions for the various slabs shown in Figs 3*b* and 4*b* (Table 3). Even though Slab 2 has Pb contents (2.76 wt.%) that are 1 wt.% lower than Pb values obtained across the profile in Fig. 4*a* (3.6–5.8 wt.%; Table 2), the rest of the short- or long-period slabs have calculated Pb values in a comparable range (3.05–5.36 wt.%; Table 3). Similarly, the Ag values obtained for mixed points along the profile in Fig. 4*a* (1.06–1.73 wt.%) are comparable to the calculated values for the slabs (1.32–2.06 wt.%). Therefore, we further stress that the mixed material in the intergrowths at the μm-scale is represented by comparable compositions at the lattice scale.

Jumps between sequences of cuprobismutite-paděraite intergrowths

In Fig. 6, we show a slip in the stacking sequence of a disordered intergrowth of paděraite ribbons in cuprobismutite. The slip defect is ~25 nm wide, consisting of seventeen 15 Å repeats. A continuous ribbon of paděraite defines the left boundary of the defect. The entire intergrowth lies in the centre of a well-ordered cuprobismutite (320 nm). The stacking sequence of units below the slip defect (from the left is: Cbs/Pad/4Cbs/Pad/2Cbs/Pad/4Cbs, and above: Cbs/Pad/Cbs/Pad/3Cbs/Pad/ 2Cbs/2Pad. On either side of the defect, the cuprobismutite lattice is regular and coherent, with minimal strain. If we ignore the first row of paděraite from the left, the layer sequences for the two chains with Pad/2Cbs 'slips' between each other within the intergrowth area are:

Slab 1 [3Cbs/Pad/2Cbs/Pad/4Cbs] (lower area on figure)

D**C**DCD**C**D**DTD**DCD**DTD**DCDCD**DTD**DCD**DTD** DCDCD**C**DCDC and

Slab 2 [Pad/3Cbs/Pad/2Cbs/2Pad] (upper area on figure)

DTDDCD**DTD**DCDCD**C**D**DTD**DCD**DTD**DCD**C**D **DTD**DCD**DTD**DCD**DTD**.

The lattice image suggests that there is a single type of 'switch' between the two slabs, with one Pad transposed into two Cbs units. Using the

TABLE 3. Calculated compositions for various strips and short/long-range slabs using mean compositions for Cbs and Pad (Table 1).

	1	2	3	4	5	6	7	8	9	10	11
Long range			Slab 1				4 × M2		Slab 2		4 × M2
Short range				Slab 3	Slab 4	Modulator 2				Modulator 2	
No of ribbons	1	61	13	7	5	6	18	1	15	5	13
Element wt.%	Mean Pad	Strip in Fig. 4*b*		(3 Cbs)	(1 Cbs)	(2 Cbs)		Mean Cbs		(2 Cbs)	
Cu	11.74	12.00	12.05	12.03	11.87	11.96	12.04	12.41	12.19	12.08	12.15
Ag	**1.00**	**1.63**	**1.74**	**1.69**	**1.32**	**1.53**	**1.71**	**2.59**	**2.06**	**1.80**	**1.98**
Fe	0.00	0.00	0.00	0.00	0.00	0.00	0.00	0.00	0.00	0.00	0.00
Cd	0.01	0.03	0.03	0.03	0.02	0.03	0.03	0.06	0.04	0.04	0.04
Pb	**6.47**	**4.29**	**3.91**	**4.09**	**5.36**	**4.62**	**4.00**	**0.91**	**2.76**	**3.69**	**3.05**
Bi	61.24	62.46	62.67	62.56	61.86	62.27	62.61	64.34	63.30	62.79	63.14
Sb	0.00	0.00	0.00	0.00	0.00	0.00	0.00	0.00	0.00	0.00	0.00
S	18.35	18.46	18.48	18.47	18.41	18.44	18.47	18.62	18.53	18.49	18.52
Te	0.04	0.03	0.02	0.02	0.03	0.03	0.02	0.00	0.02	0.02	0.02
Se	0.01	0.01	0.01	0.01	0.01	0.01	0.01	0.01	0.01	0.01	0.01
Total	98.87	98.90	98.90	98.90	98.88	98.89	98.90	98.94	98.92	98.91	98.91
Atomic proportions											
Cu	18.47	18.89	18.96	18.93	18.68	18.83	18.83	19.53	19.18	19.00	19.12
Ag	0.93	1.51	1.61	1.56	1.23	1.42	1.42	2.40	1.91	1.67	1.84
Fe	0.00	0.00	0.00	0.00	0.00	0.00	0.00	0.00	0.00	0.00	0.00
Cd	0.01	0.03	0.03	0.03	0.02		0.03	0.06	0.04	0.03	
Pb	3.13	2.07	1.89	1.97	2.59	2.23	2.23	0.44	1.33	1.78	1.47
Bi (+Sb)	29.30	29.89	29.99	29.94	29.60	29.80	29.80	30.79	30.29	30.04	30.22
S(+Te+Se)	57.29	57.60	57.66	57.63	57.45	57.56	57.56	58.09	57.82	57.69	57.78

(see text and lattice images in Figs 3*b* and 4*b*)

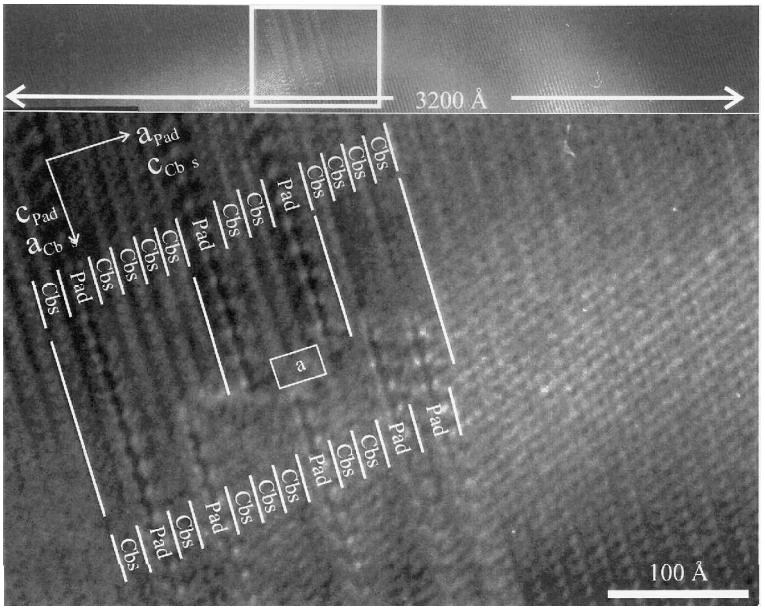

FIG. 6. A slip defect linking two different sequences of cuprobismutite (Cbs) and paděraite (Pad) cells. One of the transpositions between one Pad and two Cbs along the 17 Å repeat axis is marked as white box (a). The position of this slip within ordered Cbs is shown in the low-magnification strip at the top of the image.

structures of cuprobismutite (Ozawa and Nowacki, 1975) and paděraite (Mumme, 1986), we can model such a transformation (Fig. 7*a*) by slicing along the following chains of atoms: $(S_{19}Bi_7S_{22})_{D½T}$-$(S_{11}Bi_3S_{10}Bi_2½S_9)_{½TD}$–$(½S_9Bi_1S_8$-$S_{14})_{DC}$-$(S_{20}Bi_8S_{19})_{D½T}$ in paděraite and $(S_3Bi_4S_6S_5Bi_3½S_2)_C$–$(½S_2Bi_1½S_2)_D$-$(½S_2Bi_3S_5S_5)_C$–$(S_3Bi_2S_1)_D$ in cuprobismutite. In terms of layers, a DTD sequence in paděraite is transposed into a C layer in cuprobismutite (Fig. 7*b*). The boundary between the 2 slabs is curved, with maximum amplitude of $½a_{Cbs}$.

Replacing the groups **DTD** with *C*, the two slabs including the first paděraite row between Cbs units, become:

(1): DCD*C*DCD*C*DCD/CDCDCD*C*DCD*C*DCDCD *C*DCD*C*DCDCDCDCD/C and
(2): DCD*C*DCD*C*DCD/*C*DCD*C*DCDCDCD*C*DCD *C*DCDCD*C*DCD*C*DCD*C*.

By using the polytypic approach of Mumme (1986), we obtained similar DCDC... codes for the two chains. However, it should be mentioned that the *C*...*C* insertion in a regular DC matrix is a chemical marker for the 2 Pb atoms present in paděraite. These slip defects where paděraite ribbons can be intergrown coherently with two cuprobismutite ribbons, emphasizes the close structural relationships and modular nature of these structures.

Discussion

The data show that coherent intergrowths, at the lattice scale, between cuprobismutite and paděraite are possible along both major axes (the 15 Å and 17 Å repeat) of the two minerals. The same structural subunit, DTD, three layers of the paderaite structure, is involved in Pad/Cbs interfaces along the 15 Å repeat, as well as coherent intergrowth between Pad/2Cbs along the 17 Å repeat in slip defects.

A schematic diagram of twenty 15 Å units (30 nm), encompassing the 4 Pad$(N_{Cbs})_{1\text{-}3}$Pad slabs, is shown in Fig. 8. If we consider the intergrowths through the D layer along the 15 Å axis, the sequences represent 3 nm units of 7 layers each. If the presence of Pb is denoted by an output signal '1', and the absence of Pb by '0', then the insertion of 2 Pb in each 2D module of one paděraite unit is denoted as 101 in terms of periodic signal. The stacking of the two different mineral ribbons allow different forms of the chemical modulation signal to be expressed. The

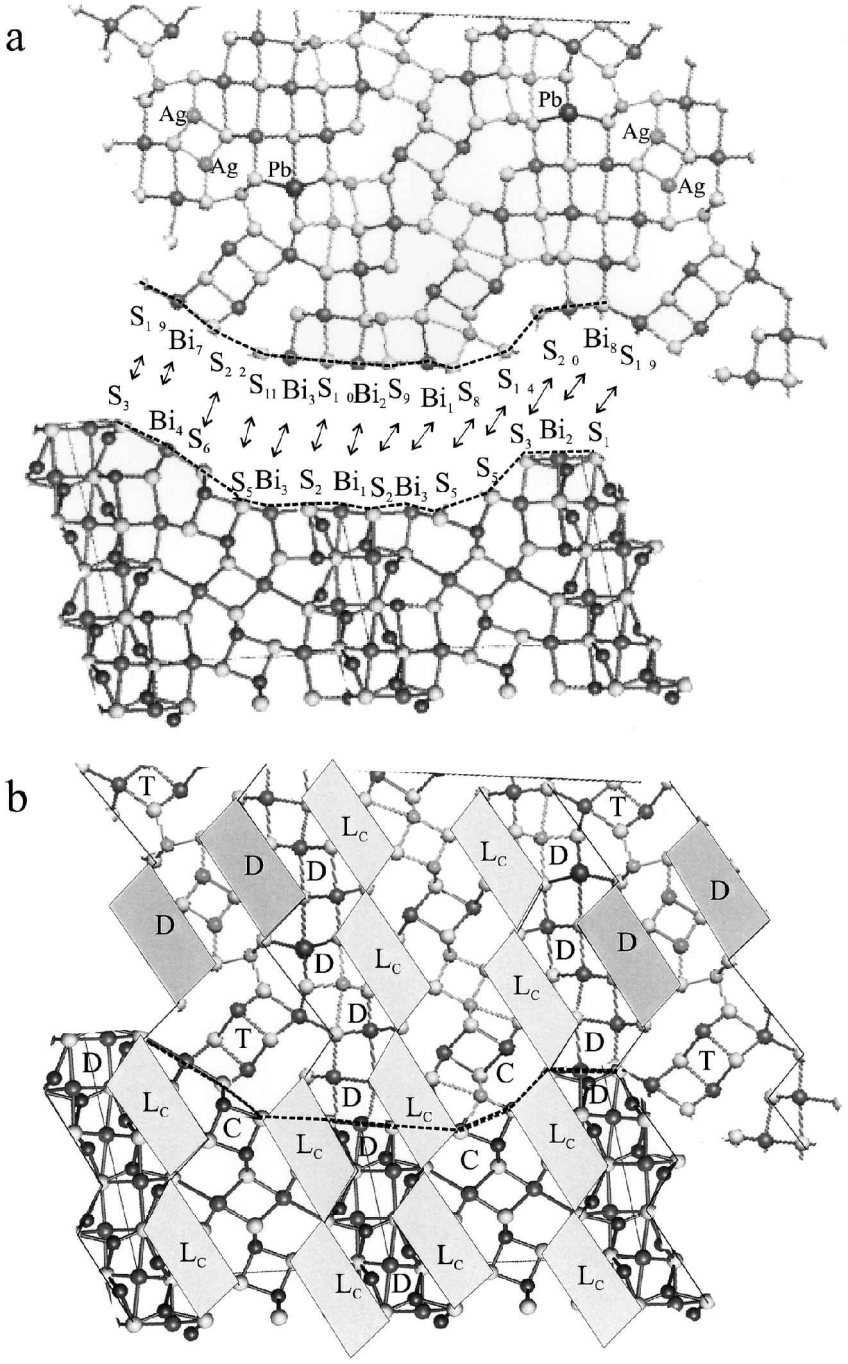

FIG. 7. Transposition along the 17 Å repeat axis of one Pad into two Cbs, as indicated by the lattice image shown in Fig. 5. (*a*) The correspondent chains of atoms in Pad and Cbs are shown using the structures of cuprobismutite (Ozawa and Nowacki, 1975) and paděraite (Mumme, 1986). (*b*) Match between the DTD_{Pad} module and C_{Cbs} across the slicing shown in (*a*). The boundary between the two slabs is curved with maximum amplitude of ½ a_{Cbs}. L_c refers to $CuBiS_{10}$ lozenges attached to the C layer (see Fig. 1).

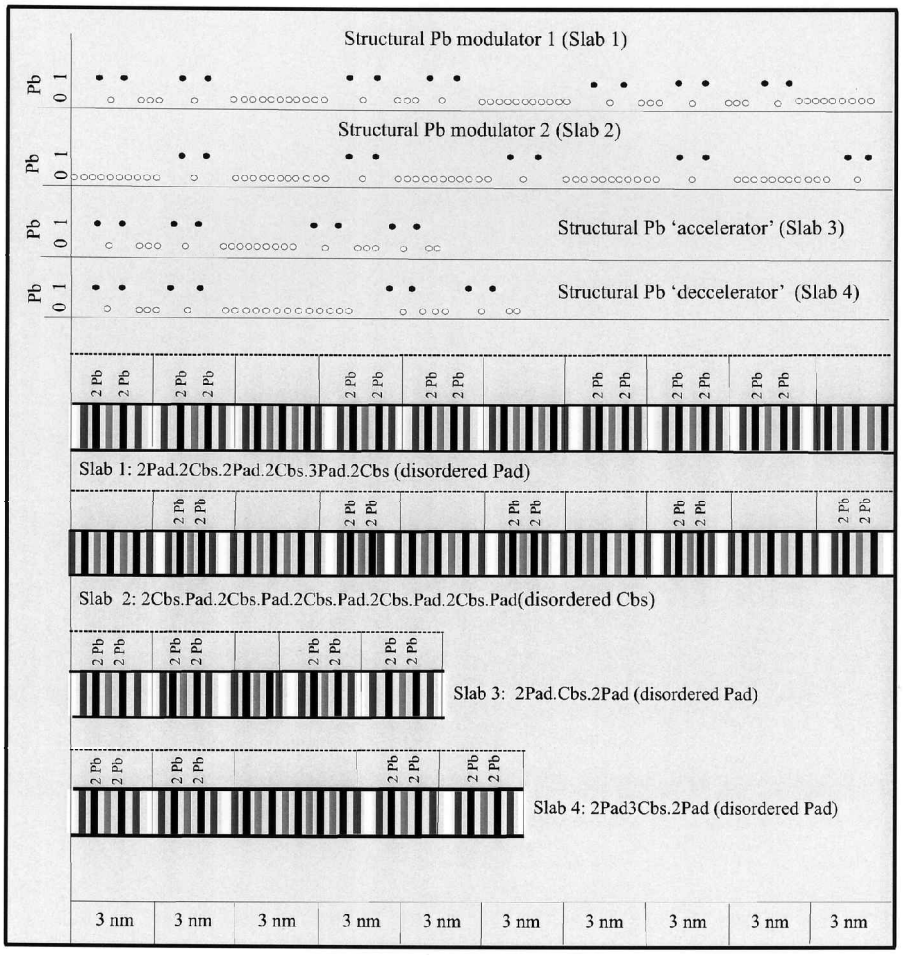

FIG. 8. Schematic diagram of slabs of coherent intergrowth between Pad and Cbs along the 15 Å repeat interpreted from the lattice images in Figs 3*b* and 4*b*. Such 'structural modulators' can be seen as long-period polysomes obtained in response to periodic chemical oscillations and local minima in free energy. The corresponding output signals realized by ordering of Pb in such polysomes are shown at the top of the figure in terms of 1 for the presence of 2Pb in D layer and 0 (gap) for the absence of Pb. These structural modulations are often thought of as being the result of long-range variation of strain in the lattice. Legend for layers: white = T; middle grey = D_{Pad} at the contact to Cbs; black = D; light grey = C.

width of the cuprobismutite slabs can have periodicities of between ×3 and ×11 layers $Pad(N_{Cbs})_{1\text{-}3}Pad$. Slab 1 (characteristic for paděraite-rich regions) modulates 101[3gaps]101[11gaps]101[3gaps]101[11gaps], whereas slab 2 (seen in more cuprobismutite-rich regions) is a regular structural modulator (for the signal 101[11gaps]101[11gaps]). By taking the two other observed N_{Cbs} (N_{Cbs} = 1,3), for example, within a paděraite slab (Fig. 8; slabs 3 and 4), we obtain the signals 101[3gaps]101[9gaps]101[3gaps]101, and 101[3gaps]101[13gaps]101[3gaps]101. Such variants of the chosen structural modulator, seen as long-period polysomes, can readily be interpreted as 'accelerators' or 'decelerators' of a variable input chemical signal. Nevertheless, the short-range polysome, containing two Cbs units positioned between Pad units (i.e. 'Modulator 2'), is the most common in the images, either in Cbs or Pad

strips. Their long-range polysomes [4 × Modulator 2] are most predictable; calculated compositions are given in Table 3.

Across the low-magnification strip in Fig. 3*b*, we see a tendency towards a banding induced by variable combinations of Pad.$(N_{Cbs})_{1\text{-}3}$.Pad modules. We can therefore interpret the lattice image as a series of irregular bands ~30 nm wide, comprising a more-or-less regular sequence of a modular 101 signal with periodic 11 gaps. To the left of the image, a group of eight PadCbsPad repeats, the presence of only one Cbs in the middle suggests that serial accelerators can occasionally occur within intervals an order of magnitude greater than the modular banding (only one within 370 nm). A comparable type of banding, realized by insertion of structural modulators of both types 1 and 2, can be seen in Fig. 4*b*. We can also see that the modulators are inserted at both boundaries of regularly stacked cuprobismutite, ~100 nm wide; further evidence for a banding tendency.

Genetic implications

The chemical oscillations are encoded in the ratios between Pad-Cbs ribbons along the stacking sequence, with period varying from one-to-three repeats of 15 Å (Fig. 8). The Pb distribution can be seen as representing an output signal that is modulated by the periodicity of stacking sequences. The Pb is carried in the D units of paděraite. In this way, the intergrowth of paděraite ribbons in the cuprobismutite matrix represents a digital type of nanoscale structural modulator for the Pb distribution. This type of polysomatic modulator acts as a patterning operator and can be activated by chemical waves with amplitudes that encompass the chemical difference between the two distinct minerals. On the other hand, conversion of the paděraite structural subunit DTD_{Pad} to the C unit of cuprobismutite, C_{Cbs}, along the 17 Å repeats, conserving the width of the interval as in Fig. 6, emphasizes that polysomatic modularity can also assist interference of chemical signals with opposite amplitudes (Fig. 9). The DTD_{Pad}/C_{Cbs} 'switchers' modulate the 'jumps' across the two different Pad-Cbs slabs at interference nodes between two chemical waves in opposite phase.

Further evidence for chemical constraints in activating the structural modulators are the μm-scale, regular, alternating intervals with compositions in the paděraite-cuprobismutite range. As noted above, the Pb gradient across a single lath in the CBP aggregates has a bimodal variation

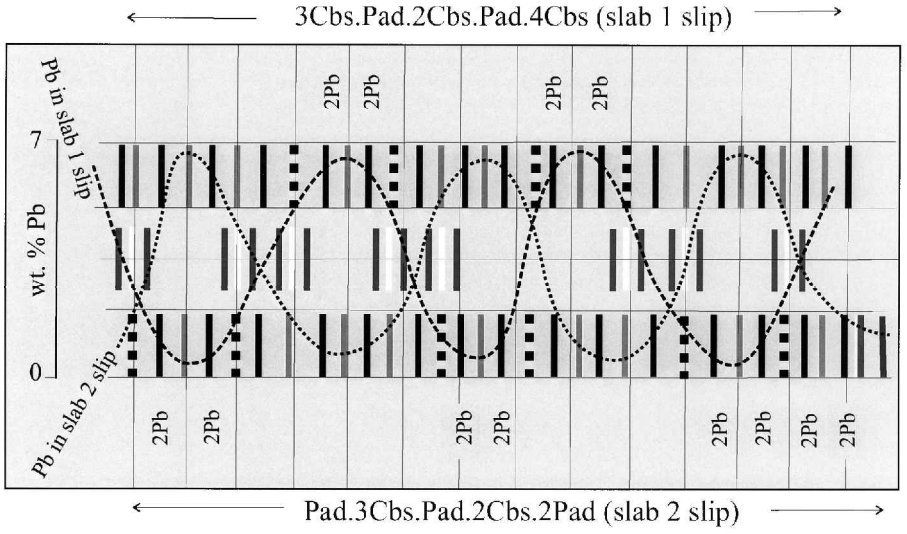

FIG. 9. Schematic representation of DTD_{Pad}/C_{Cbs} 'switchers' modulating the structural 'jumps' along the 25 nm wide slip in the stacking sequence of a disordered intergrowth of paděraite ribbons in cuprobismutite shown in Fig. 5. The legend for layers is the same as in Fig. 8. The dashed line represents the equivalent '*C*' layer for each DTD_{Pad} in the slabs. With thin dashed lines are suggested the chemical modulation as ripples with amplitude varying from one to three repeats of 15 Å along the free energy surface.

with jumps of ~3 wt.% amplitude across an interval of 5 μm. An inverse variation for Ag is coupled to the Pb variation. However, the difference in wt.% Ag between the two phases under discussion is rather small (some 1–2 wt.%), in comparison with that of Pb. The assumption that a certain minimum gradient in chemical signal is necessary to activate structural modulation is confirmed by the absence of hodrushite units in the stacking sequences, despite the fact that this mineral is occasionally present in the CBP aggregates. Hodrushite stability is controlled by the substitution ratios of Fe (Kupčik and Makovický, 1968; Koděra *et al.*, 1970). Iron may therefore represent a similar type of chemical variable for structural modularity in the cuprobismutite series. Such smaller chemical differences may nevertheless attract structural modulations in a different assemblage. As stressed, previously in our material the intermediate compositions in the 'Mix' intervals considered at the μm-scale, are observed so far only in the cuprobismutite–paděraite range.

Even though diffusion persists in sulphides to very low temperatures (e.g. Pring *et al.*, 1999), a diffusion-controlled crystallization process may be able to steadily lock in an intermediary compound in a modular series, if the free energy difference between the many possible stacking sequences were small. We believe that in these sulphosalt systems, the differences in free energy which stabilize various stacking sequences are small. Such preservation of intermediary compounds has been documented previously for minerals in the sartorite group (e.g. Pring, 2001) and also for the lillianite homologues (Pring *et al.*, 1999).

In our material, we have illustrated the type of μm-scale intergrowths that are reproduced at the nanoscale as irregular slabs of Pad-Cbs. Indeed,

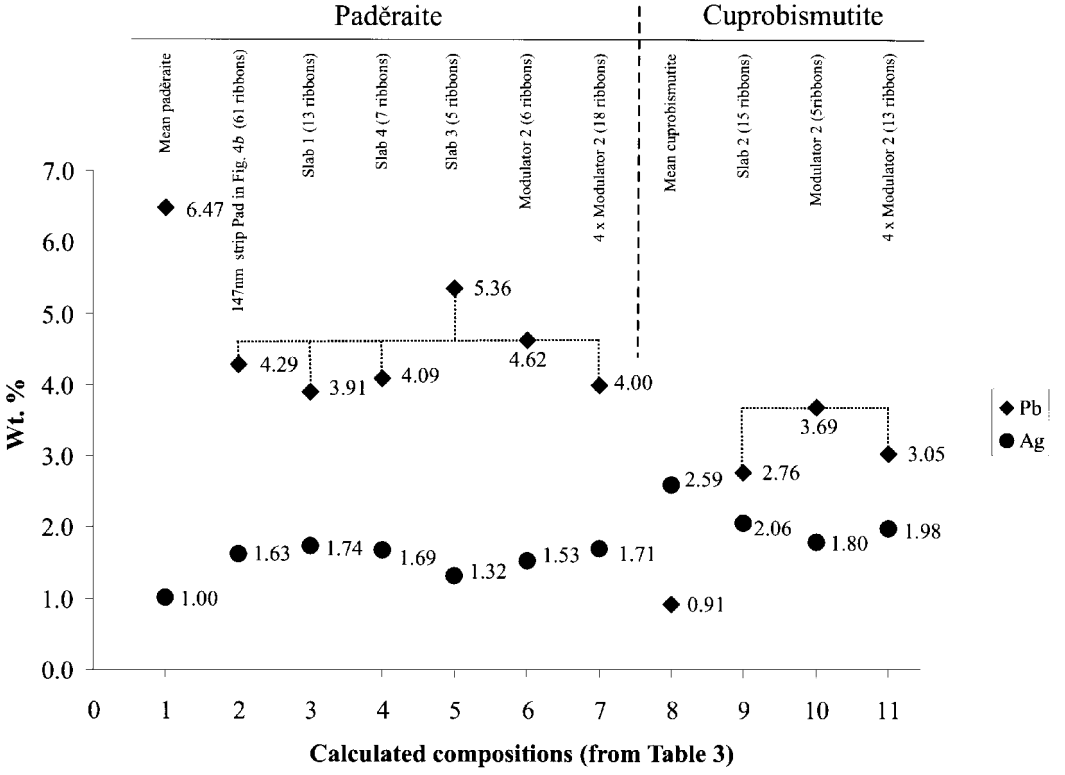

FIG. 10. Means of Pb and Ag composition (wt.%) for various short- and long-period polysomes stable within the range paděraite-cuprobismutite (discussed in the text and Table 3), as identified from the lattice images in Figs 3*b*, 4*b* and 8. They represent similar intermediate values to those obtained for the 'Mix' intervals of 5–10 μm width in the CBP (Figs 2*e*,*f* and 4*a*; Table 2). The Pb values representing the polysomes cluster around 4 wt.% Pb, irrespective of the number of ribbons they encompass.

the tendency for short-range ordering of stacking sequences and their semiperiodic occurrence in the lattice images indicates that they are the result of an oscillatory chemical signal rather than simple 'accidents' or irregular defects. Mean Pb and Ag compositions (in wt.%) for various short/long-period polysomes, stable over the paděraite-cuprobismutite range represent similar intermediate values to those obtained for the 'Mix' intervals 5–10 μm wide in the CBP (Fig. 2*e*,*f*). The Pb values representing the polysomes cluster around 4 wt.% Pb, irrespective of the number of ribbons they encompass (Fig. 10).

Coarsening of banding from the lattice- to μm-scale can be seen in the Pad-Cbs range. Such phenomena have been reported in other polysomatic series (e.g. biopyriboles; Veblen *et al.*, 1977). However, a patterning operator is required to enhance the coupling between chemical signal and structural modulation over scales differing by three orders of magnitude. One of the readily found patterning operators in a skarn environment is Liesegang banding (e.g. Ortoleva, 1994), involving an adjustment between diffusion rates and structural modulation seen in the lattice coupled to rhythmic precipitation.

The deposit at Ocna de Fier is known for its abundant rhythmic textures involving magnetite (von Cotta, 1864; Ciobanu and Cook, 2004), many of which can be interpreted as Liesegang phenomena (e.g. Kissling, 1967). The types of modular accelerators and decelerators for a chemical signal seen in Fig. 8, as well as the interference switchers in Fig. 9, are good indicators that Liesegang banding might be a suitable mechanism to explain the intergrowth-upon-intergrowth packages in our material. However, we consider that the data presented here are only a preliminary step towards a numerical model that could substantiate this hypothesis.

Acknowledgements

Funding from the South Australian Museum is gratefully acknowledged for two of us (CLC, NJC) to visit Adelaide and conduct the micro-analytical work. The senior author also gratefully acknowledges a NATO post-doctoral fellowship, focusing on the geological significance of sulphosalts, tellurides and selenides in a range of Au-bearing deposits. The assistance of Peter Self and the rest of the CEMMSA staff, Adelaide, with electron microscope operation are gratefully acknowledged. Discussions with Emil Makovicky and Dan Topa have helped us to formulate some of the ideas expressed in this paper. Constantin Gruescu is thanked sincerely for making the sample material available to us. The editor of this special issue, Chris Stanley, and an anonymous reviewer are acknowledged for their comments that helped to improve this manuscript. Lastly, we dedicate this work to the memory of Alan Criddle, with respect to his extraordinary contributions to ore mineralogy.

References

Ciobanu, C.L. and Cook, N.J. (2000) Intergrowths of bismuth sulphosalts from the Ocna de Fier Fe-skarn deposit, Banat, Southwest Romania. *European Journal of Mineralogy*, **12**, 899–917.

Ciobanu, C.L. and Cook, N.J. (2004) Skarn textures and a case study: the Ocna de Fier-Dognecea orefield, Banat, Romania. *Ore Geology Reviews*, **24**, 315–370.

Ciobanu, C.L., Cook, N.J., Topa, D., Bogdanov, K. and Merkle, R.K.W. (2002*a*) Compositional variance in the cuprobismutite series and related (Pb-bearing) paderaite: insights from new occurrences. IMA 18th General meeting, Edinburgh, *Programme with Abstracts*, p. 264.

Ciobanu, C.L., Cook, N.J. and Stein, H. (2002*b*) Regional setting and geochronology of the Late Cretaceous Banatitic Magmatic and Metallogenic Belt. *Mineralium Deposita*, **37**, 541–567.

Cook, N.J. and Ciobanu, C.L. (2003) Lamellar minerals of the cuprobismutite series and related paděraite: a new occurrence and implications. *The Canadian Mineralogist*, **41,** 441–456.

Karup-Møller, S. and Makovický, E. (1979) On pavonite, cupropavonite, benjaminite and over-substituted gustavite. *Bulletin de Minéralogie*, **102**, 351–367.

Kissling, A. (1967) Studii mineralogice şi petrografice in zona de exoskarn de la Ocna de Fier (Banat). *Editura Academiei Republicii Socialiste România*, 127 pp. (in Romanian).

Koděra, M., Kupčik, V. and Makovický, E. (1970) Hodrushite – a new sulphosalt. *Mineralogical Magazine*, **37**, 641–648.

Kupčik, V. and Makovický, E. (1968) Der Kristallstruktur des Minerals (Pb,Ag,Bi)$Cu_4Bi_5S_{11}$. *Neues Jahrbuch für Mineralogie Monatshefte*, 236–237.

Makovicky, E. (1981) The building principles and classification of bismuth-lead sulphosalts and related compounds. *Fortschritte der Mineralogie*, **59**, 137–190.

Makovicky, E. (1989) Modular classification of

sulphosalts – current status. Definition and application of homologous series. *Neues Jahrbuch für Mineralogie Abhandlungen*, **160**, 269–297.

Makovicky, E. (1997*a*) Modularity – different types and approaches. Pp. 315–343 in: *Modular Aspects of Minerals* (S. Merlino, editor). EMU Notes in Mineralogy, **1**, Eötvös University Press, Budapest.

Makovicky, E. (1997*b*) Modular crystal chemistry of sulphosalts and other complex sulphides. Pp. 237–271 in: *Modular Aspects of Minerals* (S. Merlino, editor). EMU Notes in Mineralogy, **1**, Eötvös University Press, Budapest.

Makovicky, E. and Karup-Møller, S. (1977) Chemistry and crystallography of the lillianite homologous series, Part 1. *Neues Jahrbuch für Mineralogie Abhandlungen*, **130**, 264–287.

Makovicky, E. and Makovicky, M. (1978) Representation of compositions in the bismuthinite-aikinite series. *The Canadian Mineralogist*, **16**, 405–409.

Mariolacos, K. (2002) Single crystal synthesis of the phases $Bi_{2+x}Pb_{3-x}Cu_xS_{6+x}$ and $Cu_{3-x}Bi_{5-x}Pb_{2x}S_9$ in the temperature gradient. Solid solutions in the system Bi_2S_3-PbS-Cu_2S. *Neues Jahrbuch für Mineralogie Monatshefte*, 265–275.

Mariolacos, K., Kupčik, V., Ohmasa, M. and Miehe, G. (1975) The crystal structure of $Cu_4Bi_5S_{10}$ and its relation to the structures of hodrushite and cuprobismutite. *Acta Crystallographica*, **B31**, 703–708.

Merlino, S., editor (1997) *Modular Aspects of Minerals*. EMU Notes in Mineralogy, **1**, European Mineralogical Union, 448 pp.

Mozgova, N.N. (1985) *Non-stoichiometry and Homologous Series in Sulphosalts*. Nauka, Moscow, 264 pp. (in Russian).

Mumme, W.G. (1986) The crystal structure of paděraite, a mineral of the cuprobismutite series. *The Canadian Mineraogist*, **24**, 513–521.

Mumme, W.G. and Žák, K. (1985) Paděraite, $Cu_{5.9}Ag_{1.3}Pb_{1.6}Bi_{11.2}S_{22}$, a new member of the cuprobismutite-hodrushite group. *Neues Jahrbuch für Mineralogie Monatshefte*, 557–567.

Ortoleva, P.J. (1994) *Geochemical Self-Organization*. Oxford Monographs on Geology and Geophysics **23**. Oxford University Press, Oxford, UK, 411 pp.

Ozawa, T. and Nowacki, W. (1975) The crystal structure of, and the bismuth-copper distribution in synthetic cuprobismuthinite. *Zeitschrift für Kristallographie*, **142**, 161–176.

Pring, A. (1989) Structural disorder in aikinite and krupkaite. *American Mineralogist*, **74**, 250–255.

Pring, A. (1995) Annealing of synthetic hammarite, $Cu_2Pb_2Bi_4S_9$, and the nature of cation-ordering processes in the bismuthinite- aikinite series. *American Mineralogist*, **80**, 1166–1173.

Pring, A. (2001) The crystal chemistry of the sartorite group minerals from Lengenbach, Binntal, Switzerland – a HRTEM study. *Schweizische Mineralogische Petrographische Mitteilungen*, **81**, 69–87.

Pring, A. and Etschmann, B. (2002) HRTEM observations of structural and chemical modulations in cosalite and its relationship to the lillianite homologues. *Mineralogical Magazine*, **66**, 451–458.

Pring, A. and Hyde, B. G. (1987) Structural disorder in lindströmite: a bismuthinite-aikinite derivative. *The Canadian Mineralogist*, **25**, 393–399.

Pring, A., Jercher, M. and Makovicky, E. (1999) Disorder and compositional variation in the lillianite homologous series. *Mineralogical Magazine*, **63**, 917–926.

Prodan, A., Bakker, M., Versteegh, M. and Hyde, B.G. (1982) A microscopic study of synthetic PbS-rich homologues nPbS-mBi_2S_3. *Physics and Chemistry of Minerals*, **8**, 188–192.

Skowron, A. and Tilley, R.J.D. (1986) The transformation of chemically twinned phases in the PbS-Bi_2S_3 system to the galena structure. *Chemica Scripta*, **26**, 353–358.

Skowron, A. and Tilley, R.J.D. (1990) Chemically twinned phases in the Ag_2S-PbS-Bi_2S_3 system. Part I. Electron microscope study. *Journal of Solid State Chemistry*, **85**, 235–250.

Springer, G. (1971) The synthetic solid-solution series Bi_2S_3-$BiCuPbS_3$ (bismuthinite-aikinite). *Neues Jahrbuch für Mineralogie Monatshefte*, 19–24.

Taylor, C.M., Radtke, A.S. and Christ, C.L. (1973) New data on cuprobismutite. *Journal of Research, United States Geological Survey*, **1**, 99–103.

Tilley, R.J.D. and Wright, A.C. (1982) Chemical twinning in the PbS region of the PbS-Bi_2S_3 system. *Chemica Scripta*, **19**, 18–22.

Topa, D. (2001) *Mineralogy, Crystal Structure and Crystal Chemistry of the Bismuthinite-Aikinite Series from Felbertal, Austria*. Unpublished Doctoral thesis, University of Salzburg, Austria, 249 pp.

Veblen, D.R. and Buseck, P.R. (1979) Chain-width order and disorder in biopyriboles. *American Mineralogist*, **64**, 687–700.

Veblen, D.R., Buseck, P.R. and Burnham, C.W. (1977) Asbestiform chain silicates: New minerals and structural groups. *Science*, **198**, 359–363.

von Cotta, B. (1864) *Erzlagerstätten im Banat und in Serbien*. W. Braunmuller, Wien, Austria, 105 pp.

White, T.J. and Hyde, B.G. (1982*a*) Electron microscope study of the humite minerals; I. Mg-rich specimens. *Physics and Chemistry of Minerals*, **8**, 55–63.

White, T.J. and Hyde, B.G. (1982*b*) Electron microscope study of the humite minerals; II. Mn-rich specimens. *Physics and Chemistry of Minerals*, **8**, 167–174.

Žák, L., Megarskaya, L. and Mumme, W.G. (1992) Rézbányite from Ocna de Fier (Vaskö): a mixture of bismuthinite derivatives and cosalite. *Neues Jahrbuch für Mineralogie Monatshefte*, 69–79.

Žák, L., Frýda, J., Mumme, W.G. and Paar, W.H. (1994) Makovickyite, $Ag_{1.5}Bi_{5.5}S_9$ from Báiţa Bihorului, Romania: The ^{4}P natural mineral member of the pavonite series. *Neues Jahrbuch für Mineralogie Abhandlungen*, **168**, 147–169.

[*Manuscript received 2 February 2003: revised 29 September 2003*]